nature communications

Article

https://doi.org/10.1038/s41467-025-63206-7

Shifts in precipitation regimes exacerbate global inequality in grassland nitrogen cycles

Received: 24 January 2025

Accepted: 12 August 2025

Published online: 23 August 2025

Check for updates

Miao Zheng[1,2,3], Jinglan Cui[1,2,3], Xiaoxi Wang[4,5,6], Xiuming Zhang[7], Zhongrui Xie[8], Ruoxi Zhang[2], Xinpeng Xu[8] & Baojing Gu[1,2,3]

Grasslands, the Earth's largest terrestrial ecosystem, provide crucial ecosystem services through biogeochemical cycles. However, these cycles are disrupted by climate change, particularly precipitation changes, limiting grassland productivity. By synthesizing 2944 experimental observations and integrating multiple models, here we show that under the middle-of-the-road scenario, global nitrogen input, harvest, and surplus from grasslands are projected to increase by 10, 7, and 3 million tonnes per year (Tg yr^{-1}), respectively. Substantial regional inequalities are expected. Regions with increased precipitation (mainly the United States, northern Australia, much of Asia) may see a 16 Tg yr^{-1} increase in nitrogen harvest. Conversely, regions with decreased precipitation (mainly Sub-Saharan Africa, Latin America, Southeast Asia) will see a 9 Tg yr^{-1} reduction. Timely adaptation measures could reduce nitrogen input and surplus by 12 and 22 Tg yr^{-1}, respectively, while boosting nitrogen harvest by 10 Tg yr^{-1}, potentially averting losses of 238 billion USD by 2050.

Grasslands are among the most widespread terrestrial ecosystems, covering more than 40% of Earth's land surface[1]. They provide habitats for numerous plant and animal species and play a crucial role in regulating regional and global climates[2]. Given that most grasslands are located in semi-arid areas, they are highly sensitive to changes in precipitation. Consequently, future climate change could significantly impact global grasslands. Projections indicate that global annual precipitation over land will increase by an average of 4.6% under SSP2-RCP4.5 from 2081 to 2100 compared to 1995–2014[3,4]. However, these projections reveal substantial regional variations in precipitation patterns, with some areas expected to experience increased precipitation while others may see a reduction[5–7]. Specifically, precipitation is projected to increase mainly in the northern high latitudes, including northern Asia and North America[8]. Conversely, regions such as Europe, East Asia, South Asia, and parts of South America and Africa are anticipated to experience a decrease in precipitation[3,9].

Precipitation change is a critical and complex driver, particularly due to its projected regional heterogeneity[3]. The impacts of altered precipitation regimes on grasslands may vary significantly between arid and humid regions, affecting not only productivity but also nutrient use and losses, which are closely tied to biogeochemical cycles[10–12]. The nitrogen (N) cycle is a crucial component of these biogeochemical processes in grasslands, playing a pivotal role in pasture production and carbon (C) sequestration[2]. Although air temperature and atmospheric carbon dioxide (CO_2) level also significantly affect the grassland N cycle, their distinct mechanisms and the current lack of comprehensive, integrated global datasets hinder a unified analysis. Therefore, examining individual climate drivers separately provides a necessary foundation for future integrated assessments. While climate change impacts on grassland net primary productivity (NPP) and soil organic carbon (SOC) have been extensively studied[10–12], the N cycle has received comparatively less attention[13,14]. Although previous studies have examined the effects of precipitation changes on soil N cycling[15–17], comprehensive analyses of specific N cycling variables in response to increased or decreased precipitation remain limited. It is particularly important to clarify how climate change,

[1]State Key Laboratory of Soil Pollution Control and Safety, Zhejiang University, Hangzhou, China. [2]College of Environmental and Resource Sciences, Zhejiang University, Hangzhou, China. [3]Policy Simulation Laboratory, Zhejiang University, Hangzhou, China. [4]China Academy for Rural Development, Zhejiang University, Hangzhou, China. [5]Department of Agricultural Economics and Management, School of Public Affairs, Zhejiang University, Hangzhou, China. [6]Potsdam Institute for Climate Impact Research (PIK), Potsdam, Germany. [7]International Institute for Applied Systems Analysis, Laxenburg, Austria. [8]Department of Atmospheric Sciences, School of Earth Sciences, Zhejiang University, Hangzhou, China. e-mail: bjgu@zju.edu.cn

including altered precipitation patterns, affects reactive N (N_r) emissions (all forms of nitrogen other than N_2). Excessive N_r emissions pose significant threats such as eutrophication and biodiversity loss[18–20]. The complex mechanisms of the N cycle have been recognized[21], leading to substantial modeling efforts[22,23]. However, studies linking the N cycle to climate change remain limited. Our study systematically integrates the responses of all interrelated N variables to precipitation changes from a global perspective. Meanwhile, the response of the N cycle to precipitation changes exhibits heterogeneity, potentially affecting regional development and amplifying inequalities between nations[24,25]. Due to the limited projections for global N budgets under future precipitation changes, especially concerning their monetized impacts, the integration of N cycle feedback into Earth system models (ESMs) has been delayed, affecting the accuracy and reliability of future projections.

Our study employs a meta-analysis of global precipitation experiments to enhance our understanding of how precipitation impacts grassland N cycles. We selected manipulation experiments that simulate future precipitation levels[26], providing valuable insights into the effects of altered precipitation regimes as a single climate change driver on N cycle features. In these control experiments, precipitation was the only manipulated variable, with no alterations in other factors such as air temperature or CO_2 level. Furthermore, utilizing the Model of Agricultural Production and its Impact on the Environment (MAgPIE)[27] and the Coupled Human and Nature System (CHANS)[28–31] models (Fig. S1), we project future N budgets and key C budgets of grasslands under varying precipitation scenarios and compare these projections to baseline scenarios. To accurately simulate N budgets under changing precipitation scenarios, we addressed the model's limitations using experimentally observed precipitation manipulation metadata. Recognizing that the CHANS model is also influenced by uncertainties in source data and underlying assumptions, we employed Monte Carlo uncertainty analysis to evaluate the model's predictive range. Additionally, we propose adaptation strategies designed to mitigate the adverse effects of precipitation changes on ecosystems and human well-being, evaluating the cost-benefit of these adaptation measures.

Results and discussion

Responses to precipitation changes

Our meta-analysis compiles a comprehensive dataset of 2944 response ratios (RRs) from precipitation experiments across global grasslands, providing a systematic representation of the effects of altered precipitation regimes. This dataset includes 1634 RRs for increased precipitation and 1310 RRs for decreased precipitation (Figs. S2 and S3). This meta-analysis incorporated data that conducted manipulation experiments on both managed and natural grasslands. We found that increased precipitation brings about a 26% increase in grassland NPP, with a 95% confidence interval (CI) of 19%–34%. Conversely, decreased precipitation leads to a 26% reduction (95% CI: −33% to −16%) in grassland NPP (Fig. 1). Adequate water supply enhances photosynthetic efficiency in grasslands[32]. In contrast, reduced precipitation causes water stress, prompting plants to close their stomata to minimize water evaporation. This limits CO_2 uptake, reduces photosynthetic efficiency, and decreases NPP[33–35].

Based on the aridity index (AI), defined as the ratio of total annual precipitation to potential evapotranspiration, we categorized global grasslands into arid (AI < 0.5) and humid (0.5 ≤ AI) regions[36] (Fig. S4a). Notably, the RRs of NPP to precipitation changes remain relatively stable across arid and humid regions. Under increased precipitation, NPP would increase by 30% (22%–44%) in arid regions, compared to a smaller increase of 8% (2%–15%) in humid regions (Fig. S4b). Increased precipitation directly alleviates the primary limiting factor of moisture in arid regions, thus significantly boosting plant NPP[37]. In humid regions, where water is relatively abundant, plant growth depends more on other factors such as temperature, resulting in a comparatively modest enhancement[38]. Under decreased precipitation, NPP would decline by 15% (−24% to −3%) in arid regions, compared to a

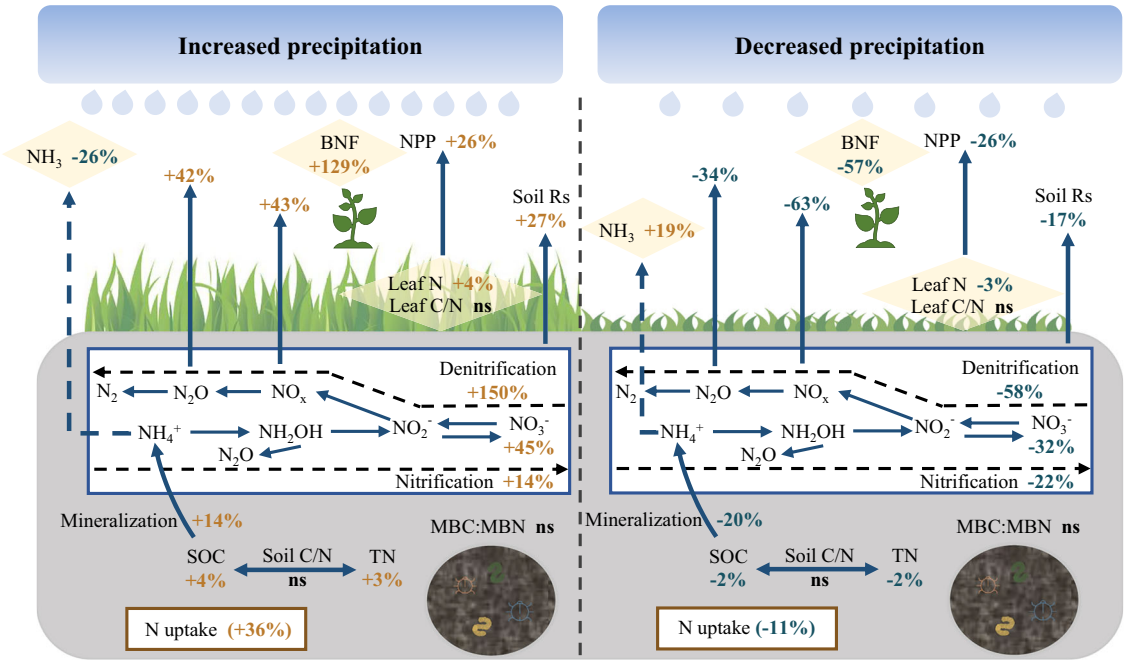

Fig. 1 | Global grassland nitrogen and carbon cycles respond to precipitation changes as a single factor. The nitrogen and carbon cycles represent the primary flows within global grasslands, depicted by blue and black lines. The percentage values in brown and green represent the increases or decreases in each nitrogen flow or store due to shifts in precipitation regimes. ns non-significant, BNF biological nitrogen fixation, NPP net primary productivity, Rs respiration, Leaf N leaf N content, Leaf C/N leaf carbon-nitrogen ratio, SOC soil organic carbon, Soil C/N soil carbon-nitrogen ratio, TN total nitrogen, MBC microbial biomass C content, MBN microbial biomass N content, N uptake nitrogen uptake. Source data are provided as a Source data file.

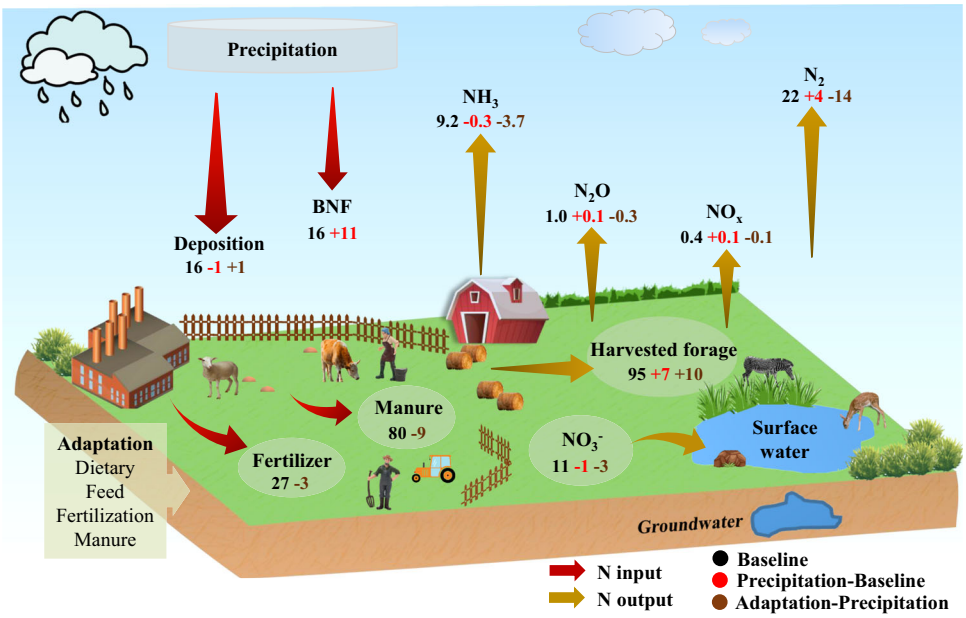

Fig. 2 | Nitrogen flows in global grasslands under the precipitation SSP2-4.5 scenario and the adaptation scenario by 2050. The nitrogen flows, including nitrogen inputs and nitrogen outputs, are illustrated by red and yellow arrows, respectively. The values of the nitrogen flows are shown in dark black for the baseline scenario with no climatic change, in red for the precipitation SSP2-4.5 scenario compared to the baseline SSP2-4.5 scenario, and in brown for the adaptation scenario relative to the precipitation scenario. In the adaptation scenario, humans implement measures such as dietary changes, efficient feed management, efficient fertilization, and efficient manure management to adapt to the precipitation conditions. These are future simulated values in Tg N per year to 2050. Source data are provided as a Source data file.

greater decrease of 29% (−39% to −19%) in humid regions (Fig. S4c). Plants in humid areas, accustomed to an adequate water supply, experience significant growth rate reductions and a substantial decline in NPP due to decreased precipitation. In contrast, plants in arid regions, adapted to low water conditions, exhibit greater drought resistance, resulting in smaller decreases in NPP[39].

Increased precipitation enhances N uptake by plants and improves the availability of N in the soil, whereas drought conditions inhibit these processes[40]. When precipitation increases, leaf N content rises by 4% (1%–8%) and total N content by 3% (1%–5%). Conversely, when precipitation decreases, leaf N content falls by 3% (−5% to −1%) and total N content by 2% (−4% to −1%) (Fig. 1). Increased precipitation also promotes soil respiration (Rs) in water-limited ecosystems[41], with Rs surging by 27% (22%–33%) under increased precipitation and decreasing by 17% (−22% to −11%) under decreased precipitation. This increase in precipitation promotes the rapid decomposition of plant residues and enhances SOC[42,43], leading to an increase in SOC by 4% (2%–6%). Conversely, decreased precipitation reduces C input from plant residues and roots, resulting in a 2% (−4% to −1%) decrease in SOC (Fig. 1). In our analysis, the C:N ratios of microbial biomass, root, litter, leaf, and soil are considered key variables for understanding the interactions between the C and N cycles, particularly in response to altered precipitation regimes (Fig. S5). The concerted variations in both the N cycle and associated losses align with the C cycle and losses in grasslands. This dynamic is reflected by the non-significant changes in soil C:N ratios, leaf C:N ratios, and microbial biomass C:N ratios.

Increased precipitation also substantially boosts biological N fixation (BNF) by 129% (78%–240%). Conversely, decreased precipitation significantly reduces BNF by 57% (−65% to −45%) (Fig. 1). This change may be related to alterations in the composition and volume of root secretions, which include rhizoctin affecting N-fixing microorganisms, thereby modifying the attachment of these microorganisms to the root system[44–46]. Enhanced precipitation also stimulates microbial activity[47], accelerating enzymatic processes such as N mineralization, denitrification, and nitrification by 14% (11%–18%), 150% (101%–218%), and 14% (11%–18%), respectively. Conversely, reduced precipitation decreases these processes by 20% (−37% to −2%), 58% (−69% to −45%), and 22% (−36% to −7%), respectively (Fig. 1). When precipitation increases, NH_3 is more likely to be retained in the soil solution in dissolved form rather than being released into the atmosphere[48], reducing NH_3 emissions by 26% (−41% to −6%). In contrast, reduced precipitation promotes NH_3 volatilization, increasing NH_3 emissions by 19% (6%–34%). Nitrous oxide (N_2O) emissions, a byproduct of both anaerobic and aerobic N conversions[49], rise by 42% (22% to 64%) with increased precipitation but fall by 34% (−48% to −17%) with decreased precipitation. Additionally, NO_x emissions increase by 43% (9%–95%) under increased precipitation, while decreasing by 63% (−72% to −48%) under decreased precipitation. The amplified nitrification due to increased precipitation results in a 45% (13%–86%) rise in NO_3^- leakage into aquatic ecosystems, whereas decreased nitrification leads to a 32% (−51% to −5%) reduction in NO_3^- leaching (Fig. 1).

Spatiotemporal variations

In our integrated model, we examine the impact of precipitation changes as a single climate change driver on N parameters, enhancing our spatial resolution to 0.5° by 0.5°. The 0.5° by 0.5° spatial resolution achieves an optimal balance between the requirement for detailed spatial granularity to capture significant regional variations. It also maintains the computational efficiency necessary for executing large-scale simulations over extended periods. The meta-analysis results primarily derive the specific parameters for each variable across different regions through meta-regression, incorporating potential moderating factors. These moderating factors include mean annual temperature (MAT), mean annual precipitation (MAP), the magnitude of precipitation change (ΔP), evapotranspiration (ET_0), solar radiation (Srad), maximum temperature (T_{max}), minimum temperature (T_{min}), and Soil C:N ratio. For each variable under altered precipitation regimes, we ensured that the regression model was statistically optimal, with the highest R^2 and the lowest corrected Akaike Information

https://doi.org/10.1038/s41467-025-63206-7

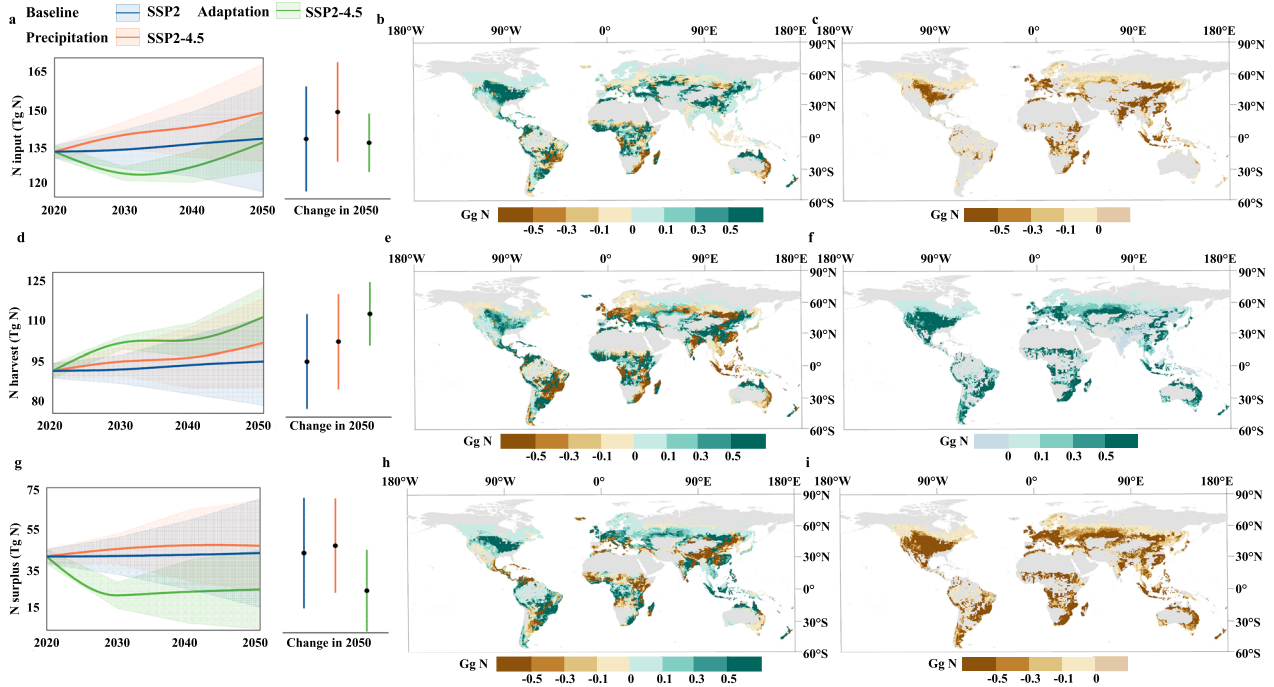

Fig. 3 | Spatiotemporal variations of global grassland nitrogen budgets change between the baseline scenario, the precipitation SSP2-4.5 scenario, and the adaptation SSP2-4.5 scenario in 2050. a Time series of nitrogen input under future scenarios over 2020-2050 in the baseline SSP2 scenario (blue), and precipitation SSP2-4.5 scenario (orange), and the adaptation SSP2-4.5 scenario (green). Solid lines represent values of nitrogen fluxes, and shadings represent standard deviations of the model ensembles of Monte Carlo simulations. **b** ΔN input between the baseline scenario and the precipitation SSP2-4.5 scenario in 2050. **c** ΔN input between the precipitation SSP2-4.5 scenario and the adaptation SSP2-4.5 scenario in 2050. Values in the legend demonstrate the average annual grassland nitrogen budget within a grid cell (0.5° by 0.5°); **d** N harvest, **e**, **f** ΔN harvest; **g** N surplus, **h**, **i** ΔN surplus. The base map is from GADM data. Source data are provided as a Source data file.

Criterion (AICc). These parameters are then applied to the model to predict future grassland N budgets under various precipitation scenarios (see "Methods," CHANS model simulation).

Our database includes both short-term and long-term experiments, with the longest study spanning up to 25 years[50]. This analysis has been effectively employed in ecosystem N budget projections[51,52]. To construct these projections, we use Representative Concentration Pathways (RCPs) and Shared Socio-economic Pathways (SSPs)[3], which form the basis for our baseline and prospective precipitation scenarios and encapsulate diverse societal, economic, and climatic conditions[53]. The projected future precipitation levels for the precipitation scenarios (SSP1-RCP2.6—"sustainable society," and SSP2-RCP4.5—"business-as-usual") relative to their respective baseline counterparts (no climate change, including warming, elevated CO_2, altered precipitation regimes, etc.—SSP1 and SSP2) are derived from the Climate Model Intercomparison Project Phase 6 (CMIP6) simulations[3] (https://esgf-node.llnl.gov/projects/cmip6/) (Fig. S6). Meanwhile, utilizing Monte Carlo simulations[54], we quantify the ensemble averages and temporal variations in grassland N budgets under a range of future climate scenarios to account for variability in meta-analysis data and models. All projected precipitation scenarios consistently show sensitivities of the N cycle to changes in precipitation, with scenarios oriented towards sustainability indicating smaller N budgets (Fig. S7).

In contrast to the baseline scenario without climate change, the precipitation SSP2-4.5 scenario predicts significant changes in global N dynamics. Total N input, N harvest, and N surplus are forecasted to increase by 10 Tg N yr^{-1}, 7 Tg N yr^{-1}, and 3 Tg N yr^{-1}, respectively (Figs. 2 and 3, Table S1). Simultaneously, the average global NUE in grasslands is expected to decline from 69% to 68% in 2050 (Fig. S8). The global grid exhibits geographical heterogeneity, and the spatial differences in N harvest and NUE changes will further deepen regional inequalities in economic development. Countries currently facing more challenges in economic development are likely to experience more negative impacts from future precipitation changes.

Projected changes in N harvest from the SSP2 scenario (92 ± 5 to 95 ± 16 Tg N yr^{-1}) to the precipitation SSP2-4.5 scenario (95 ± 5 to 102 ± 16 Tg N yr^{-1}) are projected (Fig. 3d, e). In regions with increased precipitation, N harvests are anticipated to increase by 16 Tg N yr^{-1} under the precipitation SSP2-4.5 scenario compared to the baseline SSP2 scenario by 2050 (Fig. S9a). Specifically, in global arid regions, N harvests will rise by 6.3 Tg N yr^{-1}, and in humid regions by 9.4 Tg N yr^{-1} (Fig. 4a–c). The increase in N harvests will primarily occur in the USA, northern Australia, most mid-to-high-latitude regions of Asia, and parts of Latin America and Africa. Conversely, in areas with decreased precipitation by 2050, N harvests are expected to decrease by 9 Tg N yr^{-1} (Fig. S9b). In global arid regions, N harvest is projected to fall by 2.6 Tg N yr^{-1}, and in humid regions by 6.3 Tg N yr^{-1} (Fig. 4d–f). Notably, apart from Europe, the regions witnessing significant reductions in N harvest due to decreased precipitation are predominantly low- and middle-income economies. This is especially evident in Sub-Saharan Africa, Latin America, Southeast Asia, and South Asia, where poverty and famine are ongoing issues[55]. Furthermore, the spatial changes in NUE largely mirror the changes in N harvest, with significant declines in NUE observed in areas with reduced harvests, while areas with increased harvests show minor improvements in NUE (Fig. S8).

Under the precipitation scenarios, N inputs increase from the baseline SSP2 scenario (134 ± 8 to 139 ± 21 Tg N yr^{-1}) to the precipitation SSP2-4.5 scenario (140 ± 5 to 149 ± 19 Tg N yr^{-1}). Similarly, increases are projected from the SSP1 scenario (129 ± 7 to 117 ± 18 Tg N yr^{-1}) to the precipitation SSP1-2.6 scenario (135 ± 5 to 124 ± 14 Tg N yr^{-1}) over the two decades (Figs. 3a and S7a). The variations in total N inputs across regions are primarily driven by changes in BNF and deposition. In regions with increased precipitation, areas with lower baseline precipitation, like arid zones, show more pronounced increases in N

https://doi.org/10.1038/s41467-025-63206-7

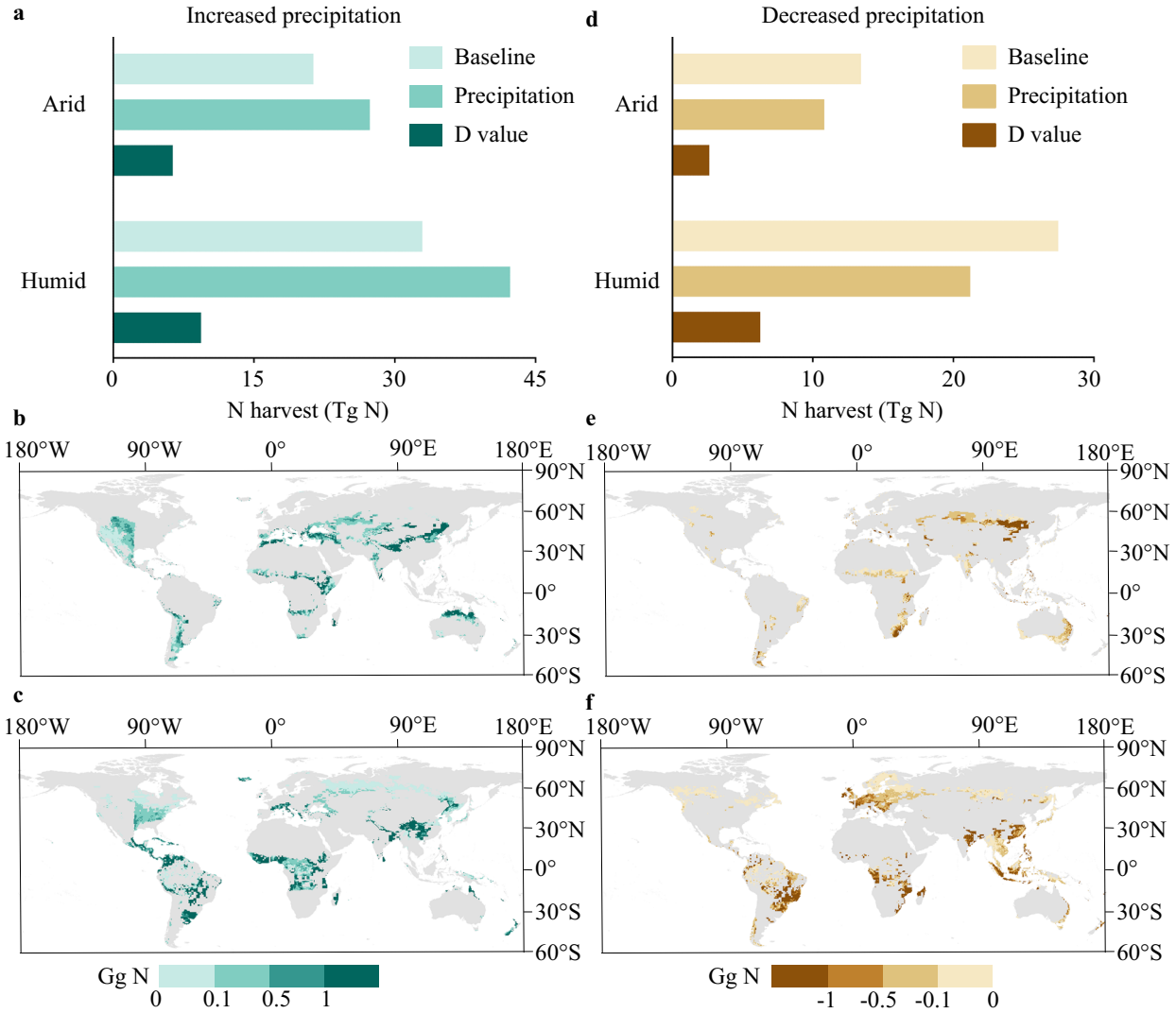

Fig. 4 | Global grassland nitrogen harvest in arid and humid regions under the precipitation SSP2-4.5 scenario compared to the baseline scenario in 2050. **a** Global grassland nitrogen harvest in arid and humid regions under increased precipitation. Light green represents the grassland nitrogen harvest in arid and humid regions under the baseline scenario in 2050 with increased precipitation. Medium green indicates the precipitation SSP2-4.5 scenario. Dark green shows the difference between the precipitation SSP2-4.5 scenario and baseline SSP2 scenario. **b** ΔN harvest in arid regions under increased precipitation. **c** ΔN harvest in humid regions under increased precipitation. **d** Global grassland nitrogen harvest in arid and humid regions under decreased precipitation. Light brown represents the grassland nitrogen harvest in arid and humid regions under the baseline scenario in 2050 with decreased precipitation. Medium brown indicates the precipitation SSP2-4.5 scenario. Dark brown shows the difference between the precipitation SSP2-4.5 scenario and baseline SSP2 scenario. **e** ΔN harvest in arid regions under decreased precipitation. **f** ΔN harvest in humid regions under decreased precipitation. Values in the legend demonstrate the average annual grassland nitrogen budget within a grid cell (0.5° by 0.5°). The base map is from GADM data. Source data are provided as a Source data file.

inputs due to enhanced water availability. Significant increases in total N inputs are projected in the USA, Mexico, northern Australia, New Zealand, and certain Latin American (Venezuela, Colombia, Argentina, Uruguay, etc.) and African regions (Central Africa, Congo, Nigeria, etc.). Moderate increases are anticipated in Europe (Italy, UK, France, etc.), China, India, Japan, and northern North America (Canada, western USA) (Fig. 3b). In contrast, in regions with decreased precipitation, humid areas experience more significant changes in N inputs. These regions, which are adapted to abundant water supplies, are more vulnerable to water stress, leading to more significant disruptions in N dynamics. Decreases are mainly concentrated in Brazil, South Africa, and eastern Australia, followed by western North America and some Asian regions. Moreover, spatial differences in N input components are observed under the precipitation SSP2-4.5 scenario (Fig. S10).

The increased N surplus includes rises in N_2O (0.1 Tg N yr^{-1}), NO_x (0.1 Tg N yr^{-1}), and non-reactive N_2 emissions to air (4 Tg N yr^{-1}), along with decreases in NH_3 (0.3 Tg N yr^{-1}) emissions to air, and NO_3^- losses to water bodies (1 Tg N yr^{-1}) (Figs. 2 and 3). NH_3 emissions rise in regions with decreasing precipitation and reduce in regions with increasing precipitation. Significant increases in NH_3 emissions are expected in Canada, Europe (UK, France, etc.), Asia (China, India, etc.), and parts of Latin America and Africa. Changes in N_2O and NO_x are relatively smaller compared to NH_3 emissions. The trend for global N_2O, NO_x, and NO_3^- losses response to precipitation changes is opposite to NH_3. Losses increase in regions like North America, Argentina, central and northern Asia, northern Australia, and central Africa. Increasing NO_3^- leaching and runoff are significant concerns, potentially aggravating eutrophication in water bodies[56]. In contrast, notable decreases are forecasted for Europe (Germany, France, UK,

https://doi.org/10.1038/s41467-025-63206-7

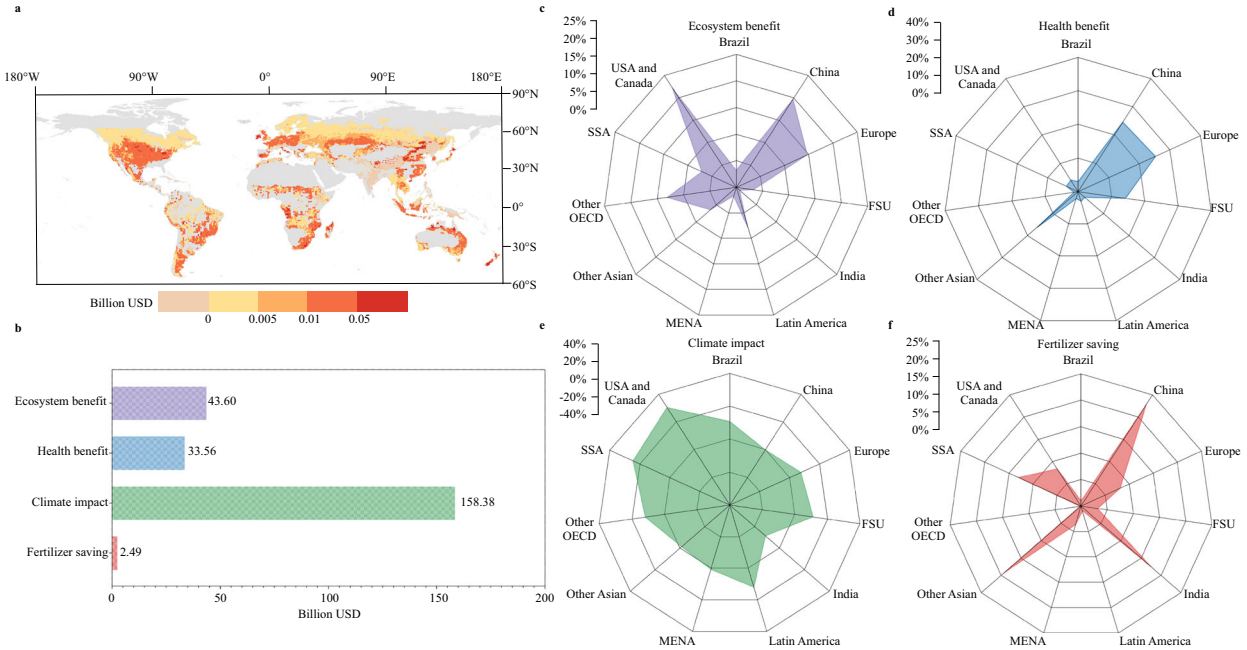

Fig. 5 | Cost-benefit analysis of precipitation levels as a single factor in global grasslands under the adaptation SSP2-4.5 scenario compared to the precipitation SSP2-4.5 scenario by 2050. a Maps display the cost-benefit analysis of adaptation to precipitation changes in global grasslands. The legend values represent the average annual grassland nitrogen budget within each grid cell (0.5° by 0.5°). The base map is from GADM data. **b** Sum of cost-benefit analysis on a global scale, comprising ecosystem benefit, human health benefit, climate impact, and fertilizer saving. **c** Percentage of global ecosystem benefit contributed by some grassland areas; **d** health benefit; **e** climate impact; **f** fertilizer saving. The positive values indicate benefits, and the negative values indicate costs. Purple represents ecosystem benefits, blue denotes human health benefits, green reflects climate impacts, and red corresponds to fertilizer savings. FSU, Former Soviet Union; Latin America, except Brazil; MENA, Middle East and North Africa; OECD, Organization for Economic Cooperation and Development; SSA, Sub-Saharan Africa. Under the precipitation SSP2-4.5 scenario (business-as-usual), changes in precipitation amounts are considered without other climate change factors. Future precipitation levels under this scenario are obtained from CMIP6 model simulations. Source data are provided as a Source data file.

etc.), southern and eastern Asia (China, India, Myanmar, Thailand, Indonesia, etc.), southern Australia, eastern Latin America (Brazil), eastern Africa, and southern Africa, followed by Canada, and northern Asia under the precipitation SSP2-4.5 scenario by 2050 (Fig. S11). In regions with increased precipitation, arid areas exhibit more substantial N surplus increases due to greater water availability. Conversely, in areas with reduced precipitation, humid regions experience more significant changes, as they are more sensitive to water shortages due to their adaptation to humid.

Adaptation scenarios and cost-benefit analysis

We develop adaptation scenarios by implementing a comprehensive set of measures across global grasslands to enhance N harvest and mitigate N pollution. Except in regions where increased N harvest and reduced N pollution occur simultaneously under precipitation scenarios, other areas need to focus on productivity enhancement or pollution reduction (Fig. S12). These measures include dietary changes, efficient feed management, efficient fertilization, and efficient manure management (Table S2). In the adaptation scenarios, these interventions are projected to significantly improve NUE[57]. Under the adaptation SSP2-4.5 scenario, NUE is expected to rise to 80%, a substantial improvement compared to the 68% forecasted in the precipitation SSP2-4.5 scenario (Fig. S8). However, socio-political barriers, such as policy limitations, technological costs, and societal willingness, may hinder achieving efficiency targets, with global cooperation being essential for their implementation[57].

A total gain of 10 Tg N yr^{-1} in N harvest would be achieved with adaptations relative to the precipitation SSP2-4.5 scenario, primarily in livestock grazing and forage production hotspots by 2050[58]. These regions include USA, Spain, France, Bulgaria, Greece, China, coastal Australia, Argentina, and Brazil under the adaptation SSP2-4.5 scenario (Fig. 3f). An increase in NUE would lead to reductions in N input and N surplus by 12 Tg N yr^{-1} and 22 Tg N yr^{-1}, respectively (Figs. 2 and 3, Table S1). Although BNF is largely governed by natural processes and less influenced by human interventions, enhanced fertilization and manure management practices[57] are predicted to reduce by 3 Tg N yr^{-1} and 9 Tg N yr^{-1}, respectively. Compared to the precipitation SSP2-4.5 scenario, the reduction in N_r losses under the adaptation SSP2-4.5 scenario is expected to be greatest in the USA, Europe, South Asia, East Asia, as well as in Africa, and Latin America. This decline in N_r losses primarily consists of decreases in NH_3 (−3.7 Tg N yr^{-1}), NO_x (−0.1 Tg N yr^{-1}), N_2O (−0.3 Tg N yr^{-1}), and NO_3^- (−3 Tg N yr^{-1}) in 2050 (Fig. 2). Collectively, these adaptation measures are projected to effectively mitigate the negative impacts of precipitation changes on grassland N dynamics.

The estimated value of the benefits from adaptation measures on global grasslands is expected to reach a considerable 238 billion US dollars under the adaptation SSP2-4.5 scenario in 2050. This valuation does not consider the costs of implementing these measures. Regionally, the largest benefits are forecasted for the USA and Canada (59 billion US dollars), Sub-Saharan Africa (44 billion US dollars), Europe (27 billion US dollars), other OECD nations (25 billion US dollars), Former Soviet Union (FSU) (24 billion US dollars), and Latin America[59] (24 billion US dollars) (Figs. 5a and S13). Most of these benefits arise from climate impact (158 billion US dollars), trailed by ecosystem benefit (44 billion US dollars), human health benefit (34 billion US dollars), and fertilizer saving (2 billion US dollars) (Fig. 5b). USA and Canada accounts for the largest share of global ecosystem benefits and climate impacts, while China contribute the most to fertilizer savings. Europe accounts for the largest share of global human health benefits

(Fig. 5c–f). Specifically, the USA and Canada are expected to achieve 10 billion US dollars in ecosystem benefits and an additional 48 billion US dollars in climate impacts. Low-income economies, including Sub-Saharan Africa, Latin America, and South and Southeast Asia, could potentially face the most severe consequences of future precipitation changes. Despite some additional costs associated with climate impacts, particularly in India and other Asian countries, the comprehensive adoption of these adaptation measures provides significant economic benefits. It also offers essential safeguards for ecosystem health, human well-being, and balanced and sustainable regional development.

Future perspective

The modification of precipitation patterns as a single driver of climate change is anticipated to alter the N cycle in global grasslands. When no appropriate measures are taken under the precipitation scenarios, our findings indicate that increased precipitation enhances forage production. This could significantly support global livestock production in the USA, northern Australia, and most mid-to-high-latitude regions of Asia. However, areas experiencing reduced precipitation may face diminished productivity, particularly in Sub-Saharan Africa, Latin America, Southeast Asia, and South Asia—regions characterized by low- and middle-income economies. These areas may struggle to meet the growing demands for food and protein of expanding human populations[60]. Additionally, the exacerbation of N_r loss due to changes in precipitation could damage atmospheric conditions, soil health, and aquatic ecosystems[61,62]. To mitigate these potential adverse effects, it is crucial to adopt sustainable and integrated management approaches. Policymakers should promote practices that ensure the efficient application of fertilizers and manure management with the changing precipitation regimes[63]. For example, using the optimal amount of fertilizer at the correct time and place is essential, coupled with the strategic integration of N inputs such as deposition and manure[64]. Simultaneously, improving the quality of forage and refining livestock feed formulas can reduce the energy requirements for feed[65], thereby minimizing N_r loss. Ongoing collaboration among scientists, pastoralists, policymakers, and the public is essential. These key stakeholders play a crucial role in developing advanced management strategies to address the global challenges posed by changing precipitation regimes.

Our study focuses on precipitation change, a critical and complex driver due to its projected regional heterogeneity[3]. While climate change encompasses multiple factors, including elevated CO_2 levels, global warming, altered precipitation patterns, and extreme weather events, all of which collectively influence grasslands[66]. It is challenging to address them comprehensively within a single study due to their distinct mechanisms and interactions. Moreover, the current lack of integrated global datasets capturing CO_2, temperature, and precipitation simultaneously limits the feasibility of integrating these variables into a unified paper. Previous research has shown that across various multifactor manipulations, elevated CO_2 level reduces root allocation, thereby diminishing the positive effects of increased air temperature and precipitation on NPP[67]. Furthermore, elevated CO_2 can mitigate the impacts of extreme droughts and heat waves on ecosystem net C uptake in the projected near-future climate[68]. Additionally, the effects of spring and non-spring precipitation on the CO_2 response offset each other, constraining the response of ecosystem productivity to rising CO_2[69]. In mesic and high-elevation grasslands, precipitation exerts a more substantial influence on soil N pools than warming does[70].

Long-term grassland responses to climate change are further shaped by factors like physiological thresholds, species interactions, acclimation, and adaptation, which can introduce nonlinearities[71–73]. These effects are context-dependent and vary with time and environmental conditions[74,75], making it difficult to extrapolate short-term results to long-term projections. Given these complexities, investigating individual climate drivers independently remains a necessary first step. Such focused studies can help build a foundation for future integrated assessments, which will benefit from improved datasets and advanced modeling approaches. As more comprehensive data and methodologies become available, we plan to explore multifactor interactions in future work. In particular, the application of century-scale models will be essential to capturing long-term dynamics of nitrogen cycling in grasslands and to informing effective adaptation and mitigation strategies under ongoing climate change.

Improving the representation of the N cycle in surface models within ESMs is crucial for understanding how climate change impacts C–N interactions in grasslands. While we assume that the effects of altered precipitation regimes will remain constant, the complexity of N cycling and the differing adaptive capacities of grassland types suggest that responses may evolve. Precipitation changes could trigger adaptive shifts in grassland species composition[11,76]. Our study focuses on the direct precipitation-productivity relationships, however, species-mediated indirect effects may also influence productivity, potentially amplifying or counteracting the direct precipitation effects. In high-latitude grasslands, slower species turnover might delay productivity responses, while in arid-to-humid transition zones, C_4 grass establishment could outweigh the benefits of increased precipitation[77]. Therefore, future research should integrate species turnover models with climate projections to better understand N cycling feedback mechanisms on grasslands under various climate scenarios. While our study operates at a global scale, more detailed attention is needed for small-scale grassland management. Furthermore, addressing the dynamic response of grasslands to multiple factors including human management and land-use change, which are worthy of future research. A comprehensive grasp of these factors and the mechanisms governing the grassland N cycle is vital for developing effective management strategies[78].

Methods

Global meta-analysis of precipitation experiments in grasslands

Most of the data used to build an extensive experimental database on variations in global precipitation came from published studies that included manipulation experiments on managed and natural grasslands, with additional soil and climate information included (Table S3). The experimental sites provide global coverage across all continents and climate zones (Fig. S3). However, due to the high financial and logistical demands of precipitation manipulation experiments, data from tropical and developing regions are limited. This lack of data may introduce uncertainties, highlighting the need for more studies in these regions in the future. We performed a cross-search to identify eligible studies based on the following criteria (see the RepOrting standards for Systematic Evidence Syntheses) flow diagram[79] added as (Fig. S14): (1) Groups exposed to ambient and changing (increased/decreased) precipitation were included in the experimental manipulations; (2) variables related to N and/or C cycles were available for these precipitation groups; and (3) these published studies are found in reliable databases such as Google Scholar, Scopus, and Web of Science. Using terms like "precipitation, rainfall, irrigation, drought," "N cycle, N fixation, NH_3, NO_x, N_2O, N runoff, N leaching, nitrification," and "C cycle, NPP, leaf N content, C:N ratio," a thorough literature search was carried out. Three main categories were gathered: research details (precipitation type, manipulation magnitude, duration, etc.), variable details (RRs, number of sample repetitions, etc.), and location specifics (country, latitude, longitude, temperature, precipitation, etc.).

Data were extracted from the figures using WebPlotDigitizer 4.4 (https://apps.automeris.io/wpd/). Additionally, missing information, particularly related to climatic and soil data, was supplemented when absent in the original publications. Climate data were primarily sourced from the WorldClim database (https://worldclim.org/data/index.html#). Soil data were obtained from the NASA Global Land Data Assimilation System (https://ldas.gsfc.nasa.gov/gldas/soils). The average AI and evapotranspiration (ET_O) were determined using datasets

from WorldClim v.2.0[80]. Climate zones were classified according to the Köppen-Geiger classification[81].

For a thorough analysis of response mechanisms to precipitation changes, we utilized multi-level meta-analyses and meta-regressions. The assessment of variables in relation to ambient precipitation levels under increased or decreased precipitation is typically conducted using the natural logarithm RR (ln$R$). The RR for an individual observation is calculated as follows[82]:

$$\ln R = \ln \alpha_{cp} - \ln \alpha_{at} \quad (1)$$

Where α_{cp} and α_{at} are the averages observed at changing (increased/decreased) and ambient precipitation levels, respectively.

Given that several papers in the dataset did not disclose the sample variance, we utilized experimental replications to weight the individual observations[82]:

$$\text{Weight} = (\omega_{cp} \times \omega_{at})/(\omega_{cp} + \omega_{at}) \quad (2)$$

Where ω_{cp} and ω_{at} represent number of experimental replications at changing (increased/decreased) and ambient precipitation levels, respectively.

The mean RR and 95% CI are obtained using a random-effects model in conjunction with a bootstrapping (4999 iterations) randomized resampling approach in MetaWin[83], with the results translated to percentage format:

$$RR\% = (e^{RR} - 1) \times 100\% \quad (3)$$

The effect of precipitation changes on the variables is deemed significant ($P < 0.05$) if the 95% CI does not include zero.

Due to the large variation in RRs, we do not use a global average for calculation. Instead, the data were categorized into the following groups: (1) individual observations, (2) arid and humid regions, (3) specific climate zones (arid, tropical, temperate, cold), and (4) global grasslands. Meta-regressions were conducted to determine global response patterns for each variable (NPP, leaf [N], BNF, NH_3, N_2O, NO_x, and NO_3^-), considering moderators that influence the geographical heterogeneity of these responses. These analyses were performed using the metafor package in R (version 4.1.3)[84]. This meta-analysis included studies with manipulation experiments on managed and natural grasslands, considering factors such as human activities. Potential moderators included MAT, MAP, and changes in precipitation magnitude (ΔP), evapotranspiration (ET_0), solar radiation (Srad), maximum temperature (T_{max}), minimum temperature (T_{min}), and soil C:N ratio. For each variable under altered precipitation regimes, we ensured that the regression model was statistically optimal, with the highest R^2 and the lowest AICc. Under increased precipitation, the RRs of NPP in arid regions and NO_3^- were adjusted based on the ΔP, while the RRs of NPP in humid regions and NO_x were influenced by the local MAP. The responses of leaf N content, BNF, and NH_3 were found to be affected by factors such as MAT, ET_0, T_{max}, and T_{min}, while the RR of N_2O in different climatic zones was incorporated into grid data. Conversely, under decreased precipitation, the RRs of these variables were adjusted based on MAT, MAP, ΔP, ET_0, Srad, T_{max}, T_{min}, and soil C:N ratio. Additionally, the RRs of leaf N content across different climatic zones were incorporated into grid data. Therefore, these parameters are not the same under different precipitation regimes. For further details, please refer to Tables S4 and S5. We also performed Monte Carlo uncertainty analyses to account for variability in the meta-analysis data.

Grassland N budget

Unlike previous studies that relied on a single model, we employed the MAgPIE[27] and CHANS[28–31] models to estimate both current and future global N budgets in grasslands, providing a more robust analysis. These estimations were carried out at a spatial resolution of 0.5° by 0.5°. The MAgPIE model provides a comprehensive global partial equilibrium land-use framework, effectively integrating regional economic conditions and biophysical methodologies (https://rse.pik-potsdam.de/doc/magpie/4.3/). CHANS represents an integrated framework that includes interactions between human activities and natural elements[28–31] (Fig. S1). It incorporates 14 subsystems, enabling it to account for various N flows and their interactions within an N mass-balance perspective, particularly well-suited to assess N cycle dynamics under varying environmental conditions. In the CHANS model, both direct N inputs (e.g., fertilizers, manure, deposition, and BNF) and N emissions from livestock production and manure management (e.g., NH_3, N_2O, N leaching, and runoff) contribute to the N budget of grasslands. The modeled N_r fluxes to the environment were validated with national monitoring data, showing a strong correlation ($R^2 > 0.7$) for air and a moderate correlation for water ($R^2 \sim 0.5$)[30]. Additionally, N harvest considers plant growth, while soil microbes facilitate the transformation and emission of N. Soil organic matter supports these processes by providing essential nutrients and enhancing microbial activity. The shared objectives of the CHANS and MAgPIE models, which are both intermediate complexity models that integrate natural and human systems, are to investigate long-term, large-scale processes of global environmental change and to identify potential solutions for mitigation and adaptation. In this research, we employed a multi-model integration strategy, incorporating MAgPIE data outputs into the CHANS model to establish global grassland N budgets. However, there is a substantial difference in the spatial resolutions of the MAgPIE and CHANS models. MAgPIE currently functions at a finer spatial resolution of 0.5° × 0.5°, in contrast to the CHANS model, which relies on country-level data for analysis. This difference suggests that integrating MAgPIE data into the CHANS model can improve the spatial resolution of simulations, enabling more detailed and localized assessments. Consequently, incorporating MAgPIE data into the CHANS model would result in improved spatial resolution for more precise localized simulations (Fig. S15). The 0.5° by 0.5° spatial resolution strikes an optimal balance, effectively reconciling the need for detailed spatial granularity to capture significant regional variations with the computational demands required for large-scale simulations over extended time periods. This model integration is grounded in their consistent application of mass-balance principles within nutrient cycle simulations. The N flows and fluxes are rigorously modeled, utilizing diverse datasets that are compatible with N balance operations. The fundamental assumptions underlying N budgeting in both models are closely aligned. According to Popp et al.'s research on forecasting future changes in grassland areas, which is based on variations in dietary habits, regional economic factors, and biophysical methods, future forage harvests will be evaluated at 10-year intervals from 2030 to 2050[53].

The N budget for grasslands can be estimated utilizing the concept of N mass balance. This involves computing the N input (N_{input}), N harvest ($N_{harvest}$), N surplus ($N_{surplus}$) and N use efficiency (NUE):

$$\sum_{x=1}^{l} N_{input,x} = \sum_{x=1}^{l} N_{harvest,x} + \sum_{x=1}^{l} N_{surplus,x} \quad (4)$$

$$NUE_x = N_{harvest,x}/N_{input,x} \quad (5)$$

$$N_{input,x} = N_{fer,x} + N_{BNF,x} + N_{man,x} + N_{dep,x} \quad (6)$$

$$N_{surplus,x} = N_{gas,x} + N_{water,x} \quad (7)$$

Where $N_{input,x}$ includes sources such as fertilizer ($N_{fer,x}$), BNF ($N_{BNF,x}$), manure ($N_{man,x}$), and deposition ($N_{dep,x}$); $N_{harvest,x}$ refers to the N

contained in the harvested forage for each grid x, primarily the leaves; $N_{surplus,x}$ encompasses N loss through gaseous emissions (NH_3, N_2O, NO_x, N_2) ($N_{gas,x}$) and N loss to water through leaching and runoff (NO_3^-) ($N_{water,x}$).

The input factor ($\theta_{input,x}$) and loss factor ($\theta_{loss,x}$) are defined as follows:

$$\theta_{input,x} = N_{input\text{-}component,x} / N_{input,x} \quad (8)$$

$$\theta_{loss,x} = N_{loss\text{-}component,x} / N_{surplus,x} \quad (9)$$

Where $N_{input\text{-}component,x}$ comprises four components: $N_{fer,x}$, $N_{BNF,x}$, $N_{man,x}$, and $N_{dep,x}$; $N_{loss\text{-}component,x}$ includes two components: $N_{gas,x}$, and $N_{water,x}$.

The reactive N ($N_{r,x}$) fluxes encompass NH_3 fluxes ($N_{NH_3,x}$), N_2O fluxes ($N_{N_2O,x}$), NO_x fluxes ($N_{NO_x,x}$), and N loss to water (NO_3^- fluxes) ($N_{water,x}$):

$$N_{r,x} = N_{NH_3,x} + N_{N_2O,x} + N_{NO_x,x} + N_{water,x} \quad (10)$$

Scenario design

To evaluate alterations in the grassland N budget due to anticipated future precipitation changes, we developed three scenarios. Firstly, the baseline scenario, which assumes no climate change and serves as a control. Secondly, the precipitation scenario, which incorporates projected changes in future precipitation patterns. Thirdly, the adaptation scenario, which considers the implementation of adaptation measures to mitigate the adverse impacts of these changes. Each scenario includes two sub-scenarios to represent distinct SSPs and RCPs (Fig. S6a). In the baseline scenario, future harvest forage demand is estimated by considering various indicators of regional economic conditions and biophysical methods[53], assuming that precipitation levels remain constant from 2020. The precipitation scenarios predict changes in precipitation levels, excluding other climate change factors such as elevated CO_2 and warming. Future precipitation levels are simulated using RCPs, such as RCP2.6 and RCP4.5 (Fig. S6b). Data on future precipitation levels (2030–2050) is derived from the CanESM5 model simulation of the WCRP Coupled Model Intercomparison Project (Phase 6; CMIP6) (https://esgf-node.llnl.gov/projects/cmip6/).

In the adaptation scenarios, a wide range of measures is implemented to effectively address N loss due to anticipated future precipitation changes. These measures encompassing dietary changes, efficient feed management, efficient fertilization, and efficient manure management would be implemented in global grasslands based on local N harvest and N_r losses conditions (Fig. S12). Dietary changes aim to ensure no country derives more than 15% of its calorie intake (29% of proteins) from animal-based foods, consistent with a "demitarian" Western dietary pattern[85], which represents a 50% reduction in the share of animal-based calories compared to current Western levels[86]. These changes may influence animal product consumption, which in turn could alter C and N cycles within grasslands, potentially leading to reduced N demand, contingent on changes in land use. To simulate these dynamics, we employed the MAgPIE model, which incorporates variations in grassland management practices and biophysical factors. Efficient feed management focuses on improving forage quality and optimizing feed compositions to reduce the energy requirements for animal feed[87]. This strategy anticipates a potential 25% reduction in feed energy needs compared to the baseline scenario, achieved through superior breeds and optimized existing feed resources. The corresponding reduction in grazing pressure may increase SOC, reduce N inputs (both fertilizer and manure), and minimize N losses, thereby improving NUE. Efficient fertilization aims to increase global fertilization efficiency from the current 60% to 75% by 2050, surpassing Europe's efficiency by fifteen percentage points and exceeding the most proficient agroecosystems[88–90]. Achieving 75% fertilization efficiency requires applying the right amount of the right fertilizer at the right time and place (4R), along with better spatial integration of heterogeneous nitrogen inputs such as atmospheric deposition and manure. Additionally, 50% of nitrogen from household waste and sewage will be recycled as fertilizers. Efficient manure management targets a 90% recycling rate for animal manure from stables to pastures by 2050, representing the highest plausible share achievable by the most efficient animal waste management systems[91–93] (Table S2).

However, socio-political barriers, including policy limitations, high implementation costs, and public willingness to adopt these measures, may pose significant challenges to reaching these efficiency targets. Addressing these barriers is crucial for realizing the improvements in our adaptation scenario, and global cooperation will be key to facilitating the implementation of these measures[57]. These measures were parameterized based on their perceived maximum potential (Table S6). We hypothesize that the implementation of these measures will enhance the management efficiency of fertilizers and manure in grasslands, ultimately resulting in a net reduction in N inputs when compared to the precipitation scenarios. Moreover, these adaptations are anticipated to increase NUE, thereby reducing N losses. By improving manure recycling and optimizing feed management, the same level of productivity can be achieved with reduced N inputs, thus minimizing N losses to the surrounding environment. For more details regarding the parameterization of the SSP1-2.6 and SSP2-4.5 adaptation scenarios, refer to Bodirsky et al.[57].

Scenario simulation

The CHANS model was employed across the above scenarios to perform N budget accounting and predict the future trajectory from 2030 to 2050, with the year 2020 serving as the baseline. In the baseline scenarios, climate change factors are excluded, and projections rely primarily on socio-economic determinants to forecast future forage harvest. These factors encompass food demand, land-use change, N fertilizer application, and livestock intensification[53]. For the precipitation scenarios, we incorporated the RRs of N cycle parameters into the CHANS model. Additionally, we refined the parameters by integrating data from various sites, allowing these scenarios to consider both socio-economic factors and anticipated changes in precipitation.

The effects of precipitation changes on total N harvest are calculated as follows:

$$N_{harvest}^{base} = \sum_{y} \left(NPP \times LeafN \times \frac{Area_{T,y}}{Area_{2020,y}} \right) \quad (11)$$

$$N_{harvest}^{precipitation} = \sum_{y} \left(NPP \times (1 + RR\%_{NPP}) \times LeafN \times (1 + RR\%_{LeafN}) \times \frac{Area_{T,y}}{Area_{2020,y}} \right) \quad (12)$$

Where $N_{harvest}^{base}$, and $N_{harvest}^{precipitation}$ represent the N harvests in the baseline and precipitation scenarios, respectively; NPP includes both aboveground and belowground NPP; Leaf N denotes the N content in leaves; $Area_{T,y}$ and $Area_{2020,y}$ signify the pasture area for the years 2030–2050 and 2020 in each baseline scenario, respectively; y signifies various regions, including REF (reforming economies of Eastern Europe and the Former Soviet Union), OECD (OECD 90 countries), Asia (Asian countries except the Middle East, Japan and Former Soviet Union states), LAM (countries of Latin America and the Caribbean), and MAF (countries of the Middle East and Africa)[53]. $RR\%_{NPP}$ and $RR\%_{Leaf\ N}$ represent the RRs of NPP and leaf N content under precipitation changes, respectively. $RR\%_{NPP}$ and $RR\%_{Leaf\ N}$ are derived by analyzing global patterns across various grids based on local climatic conditions

(Tables S4 and S5). To constrain the range of RRs, we use the highest potential NPP and the lower and upper bounds of the 95% CI obtained from meta-analysis.

In the precipitation scenario, we assume that the anthropogenic N input, such as fertilizer ($N_{fer,x}$), and manure ($N_{man,x}$) remain constant at the same level as the baseline scenario, while natural N inputs, including BNF ($N_{BNF,x}$) and N deposition ($N_{dep,x}$), are influenced by future precipitation changes. The component u of N input for BNF and deposition are susceptible to the changing (increased/decreased) precipitation.

$$N_{input,u,x}^{precipitation} = N_{input,u,x}^{base} \times (1 + RR\%_{input,u,x}) \quad (13)$$

$$\theta_{input,u,x}^{precipitation} = \frac{N_{input,u,x}^{precipitation}}{N_{input,x}^{precipitation}} \quad (14)$$

Where $RR\%_{input,u,x}$ represent the RRs of BNF and deposition for each grid x as percentage changes. $\theta_{input,u,x}^{precipitation}$ serves as key indicators for forecasting changes in grassland N budgets under different precipitation scenarios.

The effects of precipitation changes on NUE for grid x is calculated as $NUE_x^{precipitation}$:

$$NUE_x^{precipitation} = \frac{N_{harvest,x}^{precipitation}}{N_{input,x}^{precipitation}} \quad (15)$$

In the precipitation scenario, the component w of reactive N losses, including $N_{gas,x}$ and $N_{water,x}$, are influenced by future precipitation changes. The variables are calculated as follows:

$$N_{loss,w,x}^{precipitation} = N_{loss,w,x}^{base} \times (1 + RR\%_{loss,w,x}) \quad (16)$$

$$\theta_{loss,w,x}^{precipitation} = \frac{N_{loss,w,x}^{precipitation}}{N_{loss,x}^{precipitation}} \quad (17)$$

where $RR\%_{loss,w,x}$ is the RRs of reactive N loss component w under changing (increased/decreased) precipitation levels for each grid x, constrained by the 95% CIs and derived from global response patterns based on local climate conditions.

In the adaptation scenarios, global grasslands demonstrate improved NUE due to the implementation of various adaptation measures[57] (Table S2). Under the adaptation SSP2-4.5 scenario, NUE is expected to rise to 80%, a substantial improvement compared to the 68% forecasted in the precipitation SSP2-4.5 scenario. Furthermore, fertilization efficiency in grasslands has been significantly enhanced. Except in regions where increased N harvest and reduced N_r pollution occur simultaneously under precipitation scenarios, we employ a combination of adaptation measures such as dietary changes, efficient feed management, efficient fertilization, and efficient manure management for grids subjected to harvest loss or increased N pollution under the precipitation scenario (Fig. S12).

In the adaptation scenario, we assume improvements in the efficiency of fertilization and manure management due to the implementation of adaptation measures[57] (Table S2). However, natural N inputs are mainly affected by natural factors and less by adaptation measures, with BNF assumed to remain constant. Changes in response parameters related to N deposition depend on the combined emissions of NH_3 and NO_x. The N input component i includes fertilizer, BNF, manure, and deposition, as follows:

$$N_{input,x}^{adaptation} = \sum N_{input,i,x}^{adaptation} \quad (18)$$

$$\theta_{input,i,x}^{adaptation} = \frac{N_{input,i,x}^{adaptation}}{N_{input,x}^{adaptation}} \quad (19)$$

Where $\theta_{input,i,x}^{adaptation}$ serves as key indicators for forecasting changes in grassland N budgets under different adaptation scenarios.

The effects of adaptation measures on total N harvest are calculated as follows:

$$N_{harvest,x}^{adaptation} = N_{input,x}^{adaptation} \times NUE^{adaptation} \quad (20)$$

Where $N_{harvest,x}^{adaptation}$ represent the N harvests in the adaptation scenarios in grid x.

In the adaptation scenario, we assume that $\theta_{loss,w,x}$ remains constant as in the precipitation scenario.

$$N_{surplus,x}^{adaptation} = N_{input,x}^{adaptation} - N_{harvest,x}^{adaptation} \quad (21)$$

$$N_{loss,w,x}^{adaptation} = N_{surplus,x}^{adaptation} \times \theta_{loss,w,x} \quad (22)$$

Where $N_{surplus,x}^{adaptation}$ is the N surplus under the adaptation scenario in grid x; $N_{loss,w,x}^{adaptation}$ is the reactive N loss under the adaptation scenario in grid x for component w.

Cost-benefit analysis

Using the model simulation results, a cost-benefit analysis was performed utilizing global N budget data to evaluate the benefits of adaptation scenarios relative to precipitation scenarios for global grasslands. This analysis classifies countries into groups, conducting monetary evaluations at a 0.5° by 0.5° grid scale, and subsequently scales up to regional and global grasslands[31]. In the CHANS model, the anticipated costs and benefits have been distinctly allocated to grasslands, taking into account their unique N and C dynamics. Grasslands primarily rely on BNF instead of synthetic fertilizers, rendering them more vulnerable to increases in natural N inputs driven by precipitation changes. Additionally, we have considered the uneven distribution of N losses, particularly through processes such as leaching and gaseous emissions, which tend to be more pronounced in grasslands under increased precipitation. As a result, the economic and environmental costs associated with heightened N losses, including pollution and risks to biodiversity, are disproportionately higher for grasslands. Adaptation measures specific to grasslands have been modeled separately, acknowledging their lower reliance on fertilizers and distinct grazing impacts. The societal benefits associated with reducing N pollution and increasing N harvest are utilized to determine the monetized values of the adaptation measures ($C_{adaptation}$). The benefits to global grasslands encompass ecosystem benefits (C_{eco}), human health benefits (C_{human}), climate impacts ($C_{climate}$), and fertilizer savings (C_{fer}). However, there are certain costs associated with implementing these adaptation measures. These implementation costs are not factored into the cost-benefit analysis as they are considered negligible in comparison to the benefits. All benefits in this analysis are expressed in constant 2020 USD. These analyses have been validated and utilized[31,94–96]. The benefits are represented by the following equation:

$$C_{adaptation} = \sum_x (C_{eco,x} + C_{human,x} + C_{climate,x} + C_{fer,x}) \quad (23)$$

Ecosystem benefits refer to the measurable value attributed to the adverse impacts arising from changes in the N_r effects on ecosystem services. The calculation of ecosystem benefit ($C_{eco,x}$) for each grid x is determined as follows:

$$C_{eco,x} = \Delta N_{r,x} \times d_{eco,USA} \times \frac{WTP_x}{WTP_{USA}} \times \frac{PPP_x}{PPP_{USA}} \quad (24)$$

Where $\Delta N_{r,x}$ represents the changes in N_r under adaptation scenarios compared to the precipitation scenarios for grid x, including NO_3^- flows, NO_x flows, N_2O flows, and NH_3 flows; $d_{eco,USA}$ denotes the projected cost of ecosystem damage resulting from N_r losses in the United States, as estimated by Sobota et al.[97]; WTP_x and WTP_{USA} represent the relative willingness to pay for ecosystem services in grid x and the United States[98], respectively; PPP_x and PPP_{USA} indicate the purchasing power parity between the United States and grid x. To achieve comparable global ecosystem benefits, we use the ecosystem damage costs associated with N_r losses in the United States and apply them to other regions, adjusting for their willingness to pay and purchasing power parity[99]. Many cost-benefit analyses evaluating the impacts of N_r on ecosystems have been conducted in the United States and Europe[96]. However, there is currently limited data available for other regions or countries.

Human health benefits ($C_{human,x}$) refer to changes in health-related damages due to varying levels of N_r losses under future precipitation changes[97]. The monetary estimates for human health benefits are calculated using the following equation:

$$C_{huamn,x} = \Delta N_{r,x} \times d_{human,x} \quad (25)$$

Where $\Delta N_{r,x}$ denotes the variations in N_r for grid x between adaptation and precipitation scenarios, particularly NH_3 and NO_x; $d_{human,x}$ represents the health damage costs to humans from N_r loss for grid x, calculated using the N-share metric for $PM_{2.5}$ pollution, i.e., modeling with and without N_r losses to assess the contribution of N_r components to total $PM_{2.5}$ concentrations[100].

Three distinct factors are crucial in evaluating the climatic impact ($C_{climate,x}$) of precipitation changes on grasslands: C sequestration ($C_{ecc,x}$), oxygen release ($C_{eov,x}$), and N_r losses associated with climate change ($C_{N_r,x}$)[101]. We converted the changes in N harvest (calculated from NPP and leaf N content) to the value of C sequestration and oxygen release by the replacement cost method. The potent greenhouse gas N_2O significantly affects the climate in a negative way[102]. Conversely, NO_x and NH_3 are crucial as aerosol precursors, causing the reflection of long-wave solar radiation and providing a notable cooling effect on the climate system[103]. Consequently, the cost-benefit analysis of the climate impact is conducted as follows:

$$C_{climate,x} = C_{ecc,x} + C_{eov,x} + C_{N_r,x} \quad (26)$$

$$C_{ecc,x} = 1.63 \times \Delta N_{harvest,x}^{precipitation-adaptation} \times Area_x \times P_c \quad (27)$$

$$C_{eov,x} = 1.2 \times \Delta N_{harvest,x}^{precipitation-adaptation} \times Area_x \times P_{O_2} \quad (28)$$

$$C_{N_r,x} = \Delta N_{r,x} \times P_{N_r,x} \quad (29)$$

Where $C_{ecc,x}$, $C_{eov,x}$, and $C_{N_r,x}$ represent the values of C sequestration, oxygen release, and N_r in grasslands for grid x, respectively; 1.63 and 1.2 are constant parameters[104]; $\Delta N_{harvest,x}^{precipitation-adaptation}$ denotes the changes in N harvest under adaptation scenarios compared to precipitation scenarios in grid x; $\Delta N_{r,x}$ is the N_r changes for grid x; $Area_x$ represents the forage harvest area; $P_{N_r,x}$ represents the monetary valuation of the climate impact due to N_r losses for grid x, in US dollar per kg N; P_c and P_{O_2} represent the prices of C sequestration and industrial oxygen[105–107], respectively, in US dollar per kg N. The industrial oxygen price is used to approximate the value of released oxygen, as determining its exact value is challenging.

Fertilizer saving benefit ($C_{fer,x}$) pertains to the reduced investment in grassland management due to decreased synthetic fertilizer inputs under various precipitation scenarios[108]. This benefit is quantitatively determined as:

$$C_{fer,x} = \Delta N_{fer,x} \times p_{fer} \quad (30)$$

Where $\Delta N_{fer,x}$ represents the variation in N fertilizer usage under adaptation scenarios compared to precipitation scenarios for grid x; p_{fer} is the price of N fertilizer, in US dollars per kg N. Fertilizer price data are sourced from the UN Comtrade Database (https://comtrade.un.org/).

Uncertainty analysis

To assess the projected uncertainty of the grassland N budget, 1000 iterations of Monte Carlo simulations were conducted using the CHANS model[28–31]. The Monte Carlo method is a computational technique that mimics real-world conditions through random resampling, allowing for a robust analysis of variability[54]. By considering the data distribution and characteristics, the CHANS model examined the sources and magnitudes of uncertainty in the input parameters. The relative uncertainty ranges of the grassland N budget data, as well as the impact of precipitation changes on grassland N dynamics, were quantified using coefficients of variation (CV) (Table S7). After completing the 1000 simulation iterations, the means and variances of N budgets were calculated using projection ensembles.

Data availability

Data supporting the findings of this study are available within the article and its supplementary information files. A global database of precipitation simulation experiments was established by extracting data from site-based manipulation studies. The data reference generated in this study are provided in the Supplementary Information. The metadata are available under restricted access due to ongoing use in further analyses, access can be obtained upon request with the authors. Climate data were primarily sourced from the WorldClim database (https://worldclim.org/data/index.html#). Soil data were obtained from the NASA Global Land Data Assimilation System (GLDAS) (https://ldas.gsfc.nasa.gov/gldas/soils). The average AI, and evapotranspiration (ET_0) were determined using datasets from WorldClim v.2.0[80] (https://cgiarcsi.community/2019/01/24/global-aridity-index-and-potential-evapotranspiration-climate-database-v2/). Climate zones were classified according to the Köppen-Geiger classification[81]. The projected future precipitation levels for the precipitation scenarios are derived from the Climate Model Intercomparison Project Phase 6 (CMIP6) simulations[3] (https://esgf-node.llnl.gov/projects/cmip6/). Future grassland areas under different socio-economic pathways were projected from Popp et al.'s research[53]. Fertilizer price data are sourced from the UN Comtrade Database (https://comtrade.un.org/). Source data are provided with this paper.

References

1. Bai, Y. & Cotrufo, M. F. Grassland soil carbon sequestration: Current understanding, challenges, and solutions. *Science* **377**, 603–608 (2022).
2. Gruber, N. & Galloway, J. N. An Earth-system perspective of the global nitrogen cycle. *Nature* **451**, 293–296 (2008).
3. IPCC. *Climate Change 2021—The Physical Science Basis* (Cambridge Univ Press, 2021).
4. Thackeray, C. W., Hall, A., Norris, J. & Chen, D. Constraining the increased frequency of global precipitation extremes under warming. *Nat. Clim. Change* **12**, 441–448 (2022).

5. Tebaldi, C. et al. Climate model projections from the Scenario Model Intercomparison Project (ScenarioMIP) of CMIP6. *Earth Syst. Dyn.* **12**, 253–293 (2021).
6. Nie, J., Dai, P. & Sobel, A. H. Dry and moist dynamics shape regional patterns of extreme precipitation sensitivity. *Proc. Natl. Acad. Sci. USA* **117**, 8757–8763 (2020).
7. Pfahl, S., O'Gorman, P. A. & Fischer, E. M. Understanding the regional pattern of projected future changes in extreme precipitation. *Nat. Clim. Change* **7**, 423–427 (2017).
8. Zhao, J., Gan, T. Y., Zhang, G. & Zhang, S. Projected changes of precipitation extremes in North America using CMIP6 multi-climate model ensembles. *J. Hydrol.* **621**, 129598 (2023).
9. Naumann, G. et al. Global changes in drought conditions under different levels of warming. *Geophys. Res. Lett.* **45**, 3285–3296 (2018).
10. Lei, T. et al. A new framework for evaluating the impacts of drought on net primary productivity of grassland. *Sci. Total Environ.* **536**, 161–172 (2015).
11. Liu, H. et al. Shifting plant species composition in response to climate change stabilizes grassland primary production. *Proc. Natl. Acad. Sci. USA* **115**, 4051–4056 (2018).
12. Xin, X. et al. Climate change dominated long-term soil carbon losses of Inner Mongolian grasslands. *Glob. Biogeochem. Cycles* **34**, e2020GB006559 (2020).
13. Knapp, A. K. et al. Rainfall variability, carbon cycling, and plant species diversity in a mesic grassland. *Science* **298**, 2202–2205 (2002).
14. Song, J. et al. A meta-analysis of 1,119 manipulative experiments on terrestrial carbon-cycling responses to global change. *Nat. Ecol. Evol.* **3**, 1309–1320 (2019).
15. Homyak, P. M., Allison, S. D., Huxman, T. E., Goulden, M. L. & Treseder, K. K. Effects of drought manipulation on soil nitrogen cycling: a meta-analysis. *JGR Biogeosci.* **122**, 3260–3272 (2017).
16. Maxwell, T. L. et al. Contrasting drivers of belowground nitrogen cycling in a montane grassland exposed to a multifactorial global change experiment with elevated CO_2, warming, and drought. *Glob. Change Biol.* **28**, 2425–2441 (2022).
17. Wu, Q. et al. Contrasting effects of altered precipitation regimes on soil nitrogen cycling at the global scale. *Glob. Change Biol.* **28**, 6679–6695 (2022).
18. Romanelli, A., Soto, D. X., Matiatos, I., Martínez, D. E. & Esquius, S. A biological and nitrate isotopic assessment framework to understand eutrophication in aquatic ecosystems. *Sci. Total Environ.* **715**, 136909 (2020).
19. Sinha, E. & Michalak, A. M. Precipitation dominates interannual variability of riverine nitrogen loading across the continental United States. *Environ. Sci. Technol.* **50**, 12874–12884 (2016).
20. Sinha, E., Michalak, A. M. & Balaji, V. Eutrophication will increase during the 21st century as a result of precipitation changes. *Science* **357**, 405–408 (2017).
21. Niu, S. et al. Global patterns and substrate-based mechanisms of the terrestrial nitrogen cycle. *Ecol. Lett.* **19**, 697–709 (2016).
22. Davies-Barnard, T. et al. Nitrogen cycling in CMIP6 land surface models: progress and limitations. *Biogeosciences* **17**, 5129–5148 (2020).
23. Kou-Giesbrecht, S. et al. Evaluating nitrogen cycling in terrestrial biosphere models: a disconnect between the carbon and nitrogen cycles. *Earth Syst. Dyn.* **14**, 767–795 (2023).
24. Lee, M. et al. Uneven consequences of global climate mitigation pathways on regional water quality in the 21st century. *Nat. Commun.* **15**, 5464 (2024).
25. Stevens, C. J. Nitrogen in the environment. *Science* **363**, 578–580 (2019).
26. Chen, L. et al. Research advances in the soil nitrogen cycle under global precipitation pattern change. *Acta Ecol. Sin.* **40**, 7543–7551 (2020).
27. Dietrich, J. P. et al. MAgPIE 4—a modular open-source framework for modeling global land systems. *Geosci. Model Dev.* **12**, 1299–1317 (2019).
28. Gu, B., Ju, X., Chang, J., Ge, Y. & Vitousek, P. M. Integrated reactive nitrogen budgets and future trends in China. *Proc. Natl. Acad. Sci. USA* **112**, 8792–8797 (2015).
29. Gu, B. et al. Atmospheric reactive nitrogen in China: sources, recent trends, and damage costs. *Environ. Sci. Technol.* **46**, 9420–9427 (2012).
30. Gu, B. et al. Toward a generic analytical framework for sustainable nitrogen management: application for China. *Environ. Sci. Technol.* **53**, 1109–1118 (2019).
31. Gu, B. et al. Cost-effective mitigation of nitrogen pollution from global croplands. *Nature* **613**, 77–84 (2023).
32. Walther, S. et al. Satellite observations of the contrasting response of trees and grasses to variations in water availability. *Geophys. Res. Lett.* **46**, 1429–1440 (2019).
33. Ciais, P. et al. Europe-wide reduction in primary productivity caused by the heat and drought in 2003. *Nature* **437**, 529–533 (2005).
34. Xu, X., Sherry, R. A., Niu, S., Li, D. & Luo, Y. Net primary productivity and rain-use efficiency as affected by warming, altered precipitation, and clipping in a mixed-grass prairie. *Glob. Change Biol.* **19**, 2753–2764 (2013).
35. Schwalm, C. R. et al. Reduction in carbon uptake during turn of the century drought in western North America. *Nat. Geosci.* **5**, 551–556 (2012).
36. Wei, F. et al. Divergent trends of ecosystem-scale photosynthetic efficiency between arid and humid lands across the globe. *Glob. Ecol. Biogeogr.* **31**, 1824–1837 (2022).
37. Hufkens, K. et al. Productivity of North American grasslands is increased under future climate scenarios despite rising aridity. *Nat. Clim. Change* **6**, 710–714 (2016).
38. Zha, X., Niu, B., Li, M. & Duan, C. Increasing impact of precipitation on alpine-grassland productivity over last two decades on the Tibetan Plateau. *Remote Sens.* **14**, 3430 (2022).
39. Wang, B. et al. Differential effects of altered precipitation regimes on soil carbon cycles in arid versus humid terrestrial ecosystems. *Glob. Change Biol.* **27**, 6348–6362 (2021).
40. Hofer, D. *Intensively Managed Grassland Exposed to Drought–Resistance, Resilience, and Growth Limitations of Functionally Different Forage Species* (ETH Zurich, 2016).
41. Wang, Z. et al. Soil respiration response to alterations in precipitation and nitrogen addition in a desert steppe in northern China. *Sci. Total Environ.* **688**, 231–242 (2019).
42. Chen, Q., Niu, B., Hu, Y., Luo, T. & Zhang, G. Warming and increased precipitation indirectly affect the composition and turnover of labile-fraction soil organic matter by directly affecting vegetation and microorganisms. *Sci. Total Environ.* **714**, 136787 (2020).
43. Pellegrini, A. F. A. et al. Soil carbon storage capacity of drylands under altered fire regimes. *Nat. Clim. Change* **13**, 1089–1094 (2023).
44. Backer, R. et al. Plant growth-promoting rhizobacteria: context, mechanisms of action, and roadmap to commercialization of biostimulants for sustainable agriculture. *Front. Plant Sci.* **9**, 1473 (2018).
45. Pritchard, S. G. Soil organisms and global climate change. *Plant Pathol.* **60**, 82–99 (2011).
46. Nihorimbere, V., Ongena, M., Smargiassi, M. & Thonart, P. Beneficial effect of the rhizosphere microbial community for plant

growth and health. *Biotechnol. Agron. Soc. Environ.* **15**, 327–337 (2011).
47. Zhang, J. et al. Increased precipitation and nitrogen addition accelerate the temporal increase in soil respiration during 8-year old-field grassland succession. *Glob. Change Biol.* **28**, 3944–3959 (2022).
48. Deng, L. et al. Drought effects on soil carbon and nitrogen dynamics in global natural ecosystems. *Earth Sci. Rev.* **214**, 103501 (2021).
49. Wrage-Mönnig, N. et al. The role of nitrifier denitrification in the production of nitrous oxide revisited. *Soil Biol. Biochem.* **123**, A3–A16 (2018).
50. Wilcox, K. R., Blair, J. M. & Knapp, A. K. Stability of grassland soil C and N pools despite 25 years of an extreme climatic and disturbance regime. *JGR Biogeosci.* **121**, 1934–1945 (2016).
51. Cui, J. et al. Nitrogen cycles in global croplands altered by elevated CO_2. *Nat. Sustain.* **6**, 1166–1176 (2023).
52. Cui, J. et al. Elevated CO_2 levels promote both carbon and nitrogen cycling in global forests. *Nat. Clim. Change* **14**, 511–517 (2024).
53. Popp, A. et al. Land-use futures in the shared socio-economic pathways. *Glob. Environ. Change* **42**, 331–345 (2017).
54. Maia, A. G., Camargo-Valero, M. A., Trigg, M. A. & Khan, A. Uncertainty and sensitivity analysis in reservoir modeling: a Monte Carlo simulation approach. *Water Resour. Manag.* **38**, 2835–2850 (2024).
55. UNICEF. *The State of Food Security and Nutrition in the World 2024* (UNICEF, 2024).
56. Hautier, Y. et al. Eutrophication weakens stabilizing effects of diversity in natural grasslands. *Nature* **508**, 521–525 (2014).
57. Bodirsky, B. L. et al. Reactive nitrogen requirements to feed the world in 2050 and potential to mitigate nitrogen pollution. *Nat. Commun.* **5**, 3858 (2014).
58. Bengtsson, J. et al. Grasslands—more important for ecosystem services than you might think. *Ecosphere* **10**, e02582 (2019).
59. Zhang, X. et al. Managing nitrogen for sustainable development. *Nature* **528**, 51–59 (2015).
60. Tilman, D., Balzer, C., Hill, J. & Befort, B. L. Global food demand and the sustainable intensification of agriculture. *Proc. Natl. Acad. Sci. USA* **108**, 20260–20264 (2011).
61. Chaturvedi, A., Pandey, B., Yadav, A. K. & Saroj, S. Chapter 5-An overview of the potential impacts of global climate change on water resources in Water Conservation in the Era of Global Climate Change. *Elsevier* 99–120 (2021).
62. Kimmell, L. B., Fagan, J. M. & Havrilla, C. A. Soil restoration increases soil health across global drylands: a meta-analysis. *J. Appl. Ecol.* **60**, 1939–1951 (2023).
63. Oliveira, J. G. et al. Nitrogen balance and efficiency as indicators for monitoring the proper use of fertilizers in agricultural and livestock systems. *Sci. Rep.* **12**, 12021 (2022).
64. Borer, E. T., Grace, J. B., Harpole, W. S., MacDougall, A. S. & Seabloom, E. W. A decade of insights into grassland ecosystem responses to global environmental change. *Nat. Ecol. Evol.* **1**, 0118 (2017).
65. Capstaff, N. M. & Miller, A. J. Improving the yield and nutritional quality of forage crops. *Front. Plant Sci.* **9**, 535 (2018).
66. Zavaleta, E. S., Shaw, M. R., Chiariello, N. R., Mooney, H. A. & Field, C. B. Additive effects of simulated climate changes, elevated CO_2, and nitrogen deposition on grassland diversity. *Proc. Natl. Acad. Sci. USA* **100**, 7650–7654 (2003).
67. Roy, J. et al. Elevated CO_2 maintains grassland net carbon uptake under a future heat and drought extreme. *Proc. Natl. Acad. Sci. USA* **113**, 6224–6229 (2016).
68. Shaw, M. R. et al. Grassland responses to global environmental changes suppressed by elevated CO_2. *Science* **298**, 1987–1990 (2002).
69. Hovenden, M. J. et al. Globally consistent influences of seasonal precipitation limit grassland biomass response to elevated CO_2. *Nat. Plants* **5**, 167–173 (2019).
70. Lin, L. et al. Precipitation overrides warming in mediating soil nitrogen pools in an alpine grassland ecosystem on the Tibetan Plateau. *Sci. Rep.* **6**, 31438 (2016).
71. Sullivan, M. J. P., Thomsen, M. A. & Suttle, K. B. Grassland responses to increased rainfall depend on the timescale of forcing. *Glob. Change Biol.* **22**, 1655–1665 (2016).
72. Sasaki, T. et al. Dryland sensitivity to climate change and variability using nonlinear dynamics. *Proc. Natl. Acad. Sci. USA* **120**, e2305050120 (2023).
73. Williamson, J. et al. Clustered warming tolerances and the nonlinear risks of biodiversity loss on a warming planet. *Philos. Trans. R. Soc. B* **380**, 20230321 (2025).
74. Stanimirova, R. et al. Sensitivity of global pasturelands to climate variation. *Earth's Future* **7**, 1353–1366 (2019).
75. Wang, C., Vera-Vélez, R., Lamb, E. G., Wu, J. & Ren, F. Global pattern and associated drivers of grassland productivity sensitivity to precipitation change. *Sci. Total Environ.* **806**, 151224 (2022).
76. Zhu, K. et al. Rapid shifts in grassland communities driven by climate change. *Nat. Ecol. Evol.* **8**, 2252–2264 (2024).
77. Taylor, S. H. et al. Physiological advantages of C_4 grasses in the field: a comparative experiment demonstrating the importance of drought. *Glob. Change Biol.* **20**, 1992–2003 (2014).
78. Sun, J. et al. Toward a sustainable grassland ecosystem worldwide. *Innovation* **3**, 4 (2022).
79. Haddaway, N.R. et al. ROSES flow diagram for systematic maps. Version 1.0. (2017).
80. Zomer, R. J., Xu, J. & Trabucco, A. Version 3 of the global aridity index and potential evapotranspiration database. *Sci. Data* **9**, 409 (2022).
81. Beck, H. E. et al. Present and future Köppen-Geiger climate classification maps at 1-km resolution. *Sci. Data* **5**, 180214 (2018).
82. Hedges, L. V., Gurevitch, J. & Curtis, P. S. The meta-analysis of response ratios in experimental. *Ecology* **80**, 1150 (1999).
83. Rosenberg, M. S., Adams, D. C. & Gurevitch, J. MetaWin: statistical software for meta-analysis with resampling tests. (Sinauer Associates, 1997).
84. Viechtbauer, W. Conducting meta-analyses in R with the metafor Package. *J. Stat. Soft.* **36**, 1–48 (2010).
85. Sutton, M. A. et al. *Our Nutrient World: The Challenge to Produce More Food & Energy with Less Pollution* (Centre for Ecology & Hydrology, 2013).
86. Gouel, C. & Guimbard, H. Nutrition transition and the structure of global food demand. *Am. J. Agric. Econ.* **101**, 383–403 (2019).
87. Hristov, A. N. et al. Climate change effects on livestock in the Northeast US and strategies for adaptation. *Clim. Change* **146**, 33–45 (2018).
88. Bodirsky, B. L. et al. N_2O emissions from the global agricultural nitrogen cycle – current state and future scenarios. *Biogeosciences* **9**, 4169–4197 (2012).
89. DeGregori, T. R. Feeding the world: a challenge for the twenty-first century. *J. Econ. Issues* **35**, 210–212 (2001).
90. Ahmed, M. et al. Innovative processes and technologies for nutrient recovery from wastes: a comprehensive review. *Sustainability* **11**, 4938 (2019).
91. Hollas, C. E. et al. The potential of animal manure management pathways toward a circular economy: a bibliometric analysis. *Environ. Sci. Pollut. Res.* **29**, 73599–73621 (2022).
92. IPCC. *2019 Refinement to the 2006 IPCC Guidelines for National Greenhouse Gas Inventories* (Cambridge University Press, 2019).

93. IPCC. *Climate Change 2006—Guidelines for National Greenhouse Gas Inventories* (Cambridge Univ Press, 2006).
94. Zhang, X. et al. Societal benefits of halving agricultural ammonia emissions in China far exceed the abatement costs. *Nat. Commun.* **11**, 4357 (2020).
95. Zhu, Z. et al. Integrated livestock sector nitrogen pollution abatement measures could generate net benefits for human and ecosystem health in China. *Nat. Food* **3**, 161–168 (2022).
96. Van Grinsven, H. J. M. et al. Costs and benefits of nitrogen for Europe and implications for mitigation. *Environ. Sci. Technol.* **47**, 3571–3579 (2013).
97. Sobota, D. J., Compton, J. E., McCrackin, M. L. & Singh, S. Cost of reactive nitrogen release from human activities to the environment in the United States. *Environ. Res. Lett.* **10**, 025006 (2015).
98. Adekunle, M. F. Public willingness to pay for ecosystem service functions of a peri-urban forest near Abeokuta, Ogun State, Nigeria. *J. Dev. Agric. Econ.* **4**, 45–50 (2012).
99. Brink, C et al. Chapter 22-Costs and benefits of nitrogen in the environment. In *The European nitrogen assessment: Sources, effects and policy perspectives*. 513–540 (Cambridge Univ Press, Cambridge, UK 2011).
100. Gu, B. et al. Abating ammonia is more cost-effective than nitrogen oxides for mitigating $PM_{2.5}$ air pollution. *Science* **374**, 758–762 (2021).
101. Ouyang, Z. et al. Using gross ecosystem product (GEP) to value nature in decision making. *Proc. Natl. Acad. Sci. USA* **117**, 14593–14601 (2020).
102. Ravishankara, A. R., Daniel, J. S. & Portmann, R. W. Nitrous oxide (N_2O): The dominant ozone-depleting substance emitted in the 21st century. *Science* **326**, 123–125 (2009).
103. Zhang, B. The effect of aerosols to climate change and society. *J. Geosci. Environ. Prot.* **08**, 55–78 (2020).
104. Hu, X. & Lian, E. A study on accounting for the gross value of grassland ecosystems in Qinghai Province. *Qinghai Tibet Plateau Forum.* **1**, 54–59 (2022).
105. Chen, H., Costanza, R. & Kubiszewski, I. Legitimacy and limitations of valuing the oxygen production of ecosystems. *Ecosyst. Serv.* **58**, 101485 (2022).
106. Eide, L. I. et al. Enabling large-scale carbon capture, utilisation, and storage (CCUS) using offshore carbon dioxide (CO_2) infrastructure developments—a review. *Energies* **12**, 1945 (2019).
107. Costanza, R. et al. The value of the world's ecosystem services and natural capital. *Ecol. Econ.* **25**, 3–15 (1998).
108. Kanter, D. R., Zhang, X. & Mauzerall, D. L. Reducing nitrogen pollution while decreasing farmers' costs and increasing fertilizer industry profits. *J. Environ. Qual.* **44**, 325–335 (2015).

Acknowledgements

This study was supported by the National Natural Science Foundation of China (42325707 and 42261144001, B.G.; 42407480, J.C.), and Postdoctoral Fellowship Program of China Postdoctoral Science Foundation (GZC20232311, J.C.) and the Frontiers Planet Prize Award: International Champion Prize funded by the Frontiers Research. We thank Benjamin Leon Bodirsky and Michael Crawford for providing nitrogen budget data and modeling support. We thank Xiaoxiao Zhang for collection and validation of metadata.

Author contributions

B.G. and M.Z. designed the study. M.Z. conducted the research and analyzed the data. B.G. and M.Z. interpreted the findings and wrote the first draft of the paper. J.C. provided support for the study methodology. X.W. provided support for the N budget data availability. X.Z. provided support for the cost-benefit analysis. Z.X., R.Z., and X.X. provided support for metadata collection. All authors contributed to the discussion and revision of the paper.

Competing interests

The authors declare no competing interests.

Additional information

Supplementary information The online version contains supplementary material available at https://doi.org/10.1038/s41467-025-63206-7.

Correspondence and requests for materials should be addressed to Baojing Gu.

Peer review information *Nature Communications* thanks Jan Willem Erisman and the other, anonymous, reviewer(s) for their contribution to the peer review of this work. A peer review file is available.